Failure criterion for composite structure with an open-hole or bolted joint using characteristic volume approach

Arruck Tragangoon[1], **Baramee Patamaprohm**[2], **Jacques Renard**[1], **Vladimir Gantchenko**[1], **Xavier Cerrillo**[3]

1. *Centre des matériaux P.M.-Fourt, Mines-Paris Tech, CNRS UMR 7633, BP 87, 91003 Evry cedex, France*
   arruck.tragangoon@mines-paristech.fr

2. *Department of Mechanical and Aerospace Engineering, DMIE Center, King Mongkut's University of Technology North Bangkok, 1518 Pibulsongkram Road, Bangsue, Bangkok 10800, Thailand*

3. *Faurecia, Z.I. Brières-les-Scellés, BP 89, 91152 Étampes cedex, France*

ABSTRACT. *We propose a non-local failure criterion to predict the failure of composite laminated structures submitted to local stress concentration. The twill glass/polyamide 6 composite specimens with an open-hole as well as a bolted joint have been investigated. Material behavior was modeled using Hill's yield criterion to describe its anisotropic non-linearity. To determine a structure failure, based on the classical characteristic distance approach, the proposed method predicts the structure failure using the characteristic volume identified by experimental testing and numerical simulations. The average values of failure criteria indices over this characteristic volume were used to determine the failure. The damage initiations were predicted and showed a good agreement with the experimental results.*

RÉSUMÉ. *Ce travail présente une prédiction de la rupture d'une structure en composite tissé en utilisant une approche non locale. Le matériau de l'étude est un composite thermoplastique renforcé par un tissu de verre sergé. Le comportement anisotrope et la non-linéarité du matériau ont été modélisés en utilisant le critère de Hill. Afin de déterminer la rupture d'une structure, l'utilisation d'un volume critique, fondé sur l'approche d'une distance critique, a été adoptée. La géométrie de ce volume critique est identifiée à l'aide d'essais expérimentaux et de calculs numériques. La valeur moyenne du critère de rupture sur ce volume critique est utilisée pour déterminer la rupture. Les charges prédites sont en bon accord avec les résultats expérimentaux.*

KEYWORDS: *holed woven composite, non-local failure criterion, characteristic volume/area, bolted assembly.*

MOTS-CLÉS : *composite tissé avec trou, critère de rupture non local, volume/aire caractéristique, assemblage boulonné.*

DOI: 10.3166/rcma.2017.00026

1. Introduction

Recently, automotive industry has been focusing on weight reductions with an idea of replacing several metallic parts with composites due to their favorable high mechanical properties to weight ratio. In particular, for the woven composites, a good resistance to delamination is an additional advantage. In industrial structural applications, the composites with open holes or mechanical joint are very common. As proposed by Nelson *et al*. (1983), the efficiency of a bolted composite joint is lower than the bolted metal joint due to the different behavior in crack and damage initiation as well as its propagation. In 2000, Duthinh (2000) found that the stress concentration at a circular hole is significantly larger in fiber-reinforced composites than in ductile metals, and that metal plasticity relieves the stress concentration around the hole unlike fiber-reinforced composites. In order to predict the strength of composite laminates with stress concentration due to the presences of holes, many approaches have been proposed. Each of them has its own advantages. The well-known point stress and average stress proposed by Whitney and Nuismer (1974) are the characteristic distance approach, which is widely used in the industry due to its simplicity. Based on this classic method, many authors proposed modifications, for example, effective stress fracture models which utilize a characteristic length (Tan, 1988), a characteristic length based on FEM with progressive damage approach (Wang *et al*., 2004). Recently, some authors proposed a characteristic volume approach (Hochard *et al*., 2007; Miot *et al*., 2010), which is practical to apply due to its less geometry-dependence. Moreover, this characteristic volume approach has been also proposed for the bearing failure onset of pin-contact in composite laminates (Wu and Sun, 1998), while some authors has been proposed failure area index method (Choi and Chun, 2003) which predicts the failure from an average value of failure indices of damaged elements.

In this work, we proposed a non-local failure criterion for composites with an open hole or a bolted composite join. The mechanical properties of composite laminate were determined experimentally. Then, experimental tests were conducted on open-hole specimens to identify the parameter of the proposed method semi-empirically, and also to validate the proposed method. Then, the mechanical tests on the bolted composite join were carried out in order to determine the failures of the joins, which were used to validate the proposed method in predicting the bolted join failure. Finally, the application of the proposed method on the industrial structure was also presented.

2. Non-local approach

For composite materials, when stress field is non-uniform induced by any stress concentrations, the failure criteria locally applied on a structure would result in an underestimated failure load. As pointed out by many authors, the structure failure does not occur immediately after minor failure but after failure of a sufficient volume. Due to this fact, the failure prediction using characteristic length has been proposed. This length needs to be determined experimentally. However, since the characteristic length is

rather sensitive to geometry variation, the method proposed in this work uses a characteristic volume to determine the failure of structures under loading.

The shape of characteristic volume was chosen to be cylindrical which reduces the effect of stress singularity at a holed edge and has only diameter and thickness to be identified.

The failure of structure is obtained when an average value of interested quantity over the characteristic volume is satisfied. The calculated average value can be stress components or failure criteria's indices. In this work, the selected failure criteria were the maximum stress criterion and Hashin failure criteria, which is originally proposed for unidirectional composites. Some failure modes of Hashin were chosen to be applied on woven composites as described in the following section. The parameters of these failure criteria have been determined at each point in the material considered in the characteristic volume, and then averaged over this volume as followed:

$$\overline{FI} = \frac{1}{V}\int_V FI \cdot dv \tag{1}$$

where FI stands for local failure index, $\overline{FI}$ is the average failure index over characteristic volume.

3. Modeling of material behavior

Material investigated in this work is a twill glass/polyamide 6 composite balanced in warp and weft with volume fraction of 45%. The laminates have a thickness of 2 mm (four plies in total). In order to determine material elastic constants, including three Young's moduli, three shear moduli, and three Poisson's ratios, mechanical tests including tensile, compressive, bending and Arcan-Mines tests have been carried out.

To determine the in-plane mechanical properties, the tensile tests were performed in three material's orientations; warp direction (0°), weft direction (90°), and off-axis direction (45°), according to ASTM D3039 on the universal test machine Instron 5982 with crosshead speed of 1 mm/min. Longitudinal and transversal strains were measured by AVE (Advanced Video Extensometer) and mechanical extensometers as shown in figure 1.

In order to establish the failure criterion for general application, the compressive strength has to be determined. The compressive tests were performed only in the warp direction due to material availability, while assuming that the mechanical properties of the warp and weft directions are identical. The testing procedure according to ASTM D6641 was followed using the crosshead speed of 1.3 mm/min. Each specimen was equipped by a strain gauge on each faces to measure the strain and to detect the buckling of specimen. The specimen displacements were also measured by AVE, as shown in figure 2.

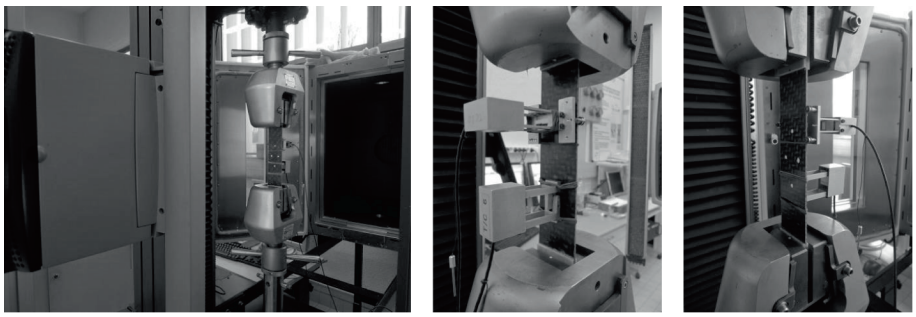

(a) (b) (c)

Figure 1. Experimental setup for tensile tests: (a) using two observation methods; (b) longitudinal and transversal extensometers; (c) AVE four observation points

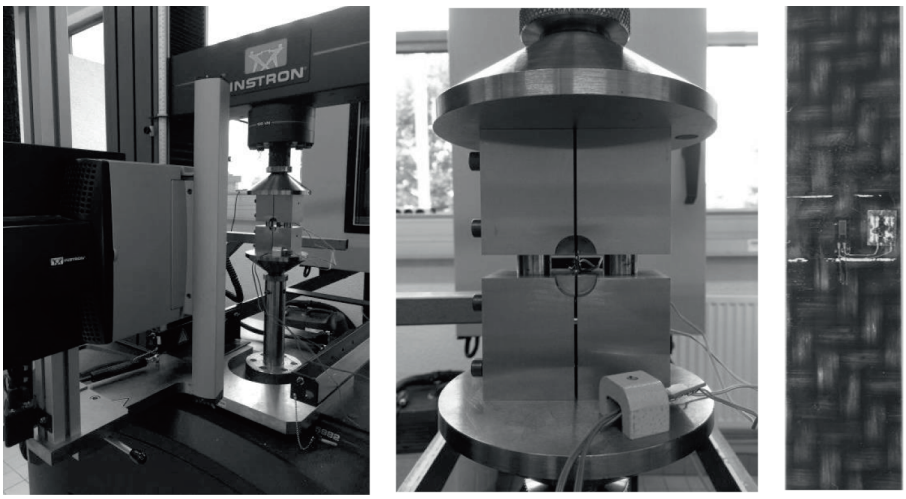

(a) (b) (c)

Figure 2. Experimental setup for compressive tests: (a) displacement observed by AVE; (b) boundary specimen fixed according to ASTM D6641; (c) each specimen is equipped by a strain gauge on each face

The three-point bending tests were also carried out using a specific setup to determine shear moduli and shear strengths in the out of plane direction. The experiments were guided by ISO 14125 with the crosshead speed of 1 mm/min. The displacements were measured by AVE, as shown in figure 3.

In order to determine the out of plane Young's modulus and failure strength, the Arcan-Mines tests were performed. Since the measured deformation is the contribution of deformation from a sandwich-structure specimen including metal substrates, adhesive, and composite (figure 4). Given the mechanical behaviors of metals substrates

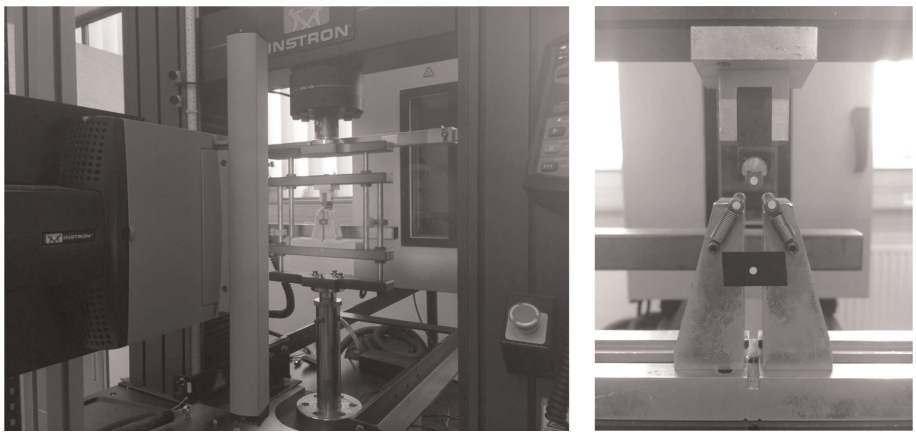

Figure 3. Displacements measured by AVE

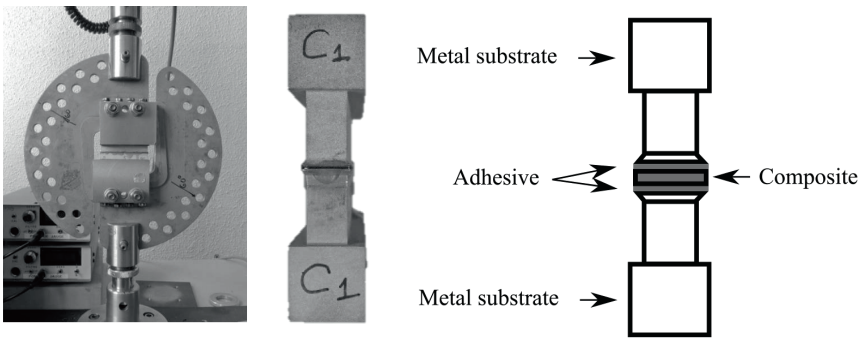

Figure 4. Arcan-Mines tests: (a) experimental setup for tensile tests in the out of plane direction; (b) Arcan-Mines test specimen; (c) sandwich-structure of the Arcan-Mines test specimen

and adhesive, the out of plane mechanical properties of composite can be semi-empirically determined by the simulation of entire Arcan-Mines tests including the grips and the sandwich-structure specimen (Patamaprohm *et al*., 2016).

Finally, in order to complete the stiffness matrix, the Poisson's ratios ν_{13} and ν_{23} were also determined. Since these mechanical properties are difficult to measure due to a small thickness of the composite sheet, the Poisson's ratios ν_{13} and ν_{23} were estimated by the rule of mixtures. From the literatures, the Poisson's ratio concerning the matrix polyamide 6 is 0.39 (Rösch, 1995) and 0.037 for out of plane direction of a woven fabric (Gay, 2005). Given that the fiber volume fraction V_f is 45% and the Poisson's ratios ν_{13} and ν_{23} are identical, we obtained:

Table 1. Results of tensile, compressive, and bending test

E_1[a] (GPa)	E_2 (GPa)	E_3 (GPa)	ν_{12}	ν_{13}	ν_{23}	G_{12} (GPa)	G_{13} (GPa)	G_{23} (GPa)
20.65	22.14	4.00	0.07	0.23	0.23	2.96	1.60	1.67
[a]E_1 in compression is 23.15 GPa.								
S_{11T} (MPa)	S_{11C} (MPa)	S_{22T} (MPa)	S_{22C}[b] (MPa)	S_{33} (MPa)	S_{12} (MPa)	S_{13} (MPa)	S_{23} (MPa)	
447.65	360.94	434.19	360.94	15.62	119.83	43.3	41.21	
[b]S_{22C} is assumed to be equal to S_{11C} due to material availability								

$$\nu_{13} = \nu_{23} = (1 - V_f)\nu_{\text{matrix}} + V_f \nu_{fabric} = 0.23 \quad (2)$$

The results of mechanical properties are summarized in the table 1, where S is the material strength and subscripts T and C stand for tensile and compressive properties, respectively. The material responses from tensile tests obviously show the characteristic of the balanced woven composite (figure 5), where the linear response up to failure was found in both fiber directions (0° and 90° directions). In the 45° direction, a non-linear response was found as a result of plasticity of matrix, microdamages, and fiber reorientations toward loading direction. This non-linearity exists only in the off-axis directions, which is contributed by the in-plane shear stress.

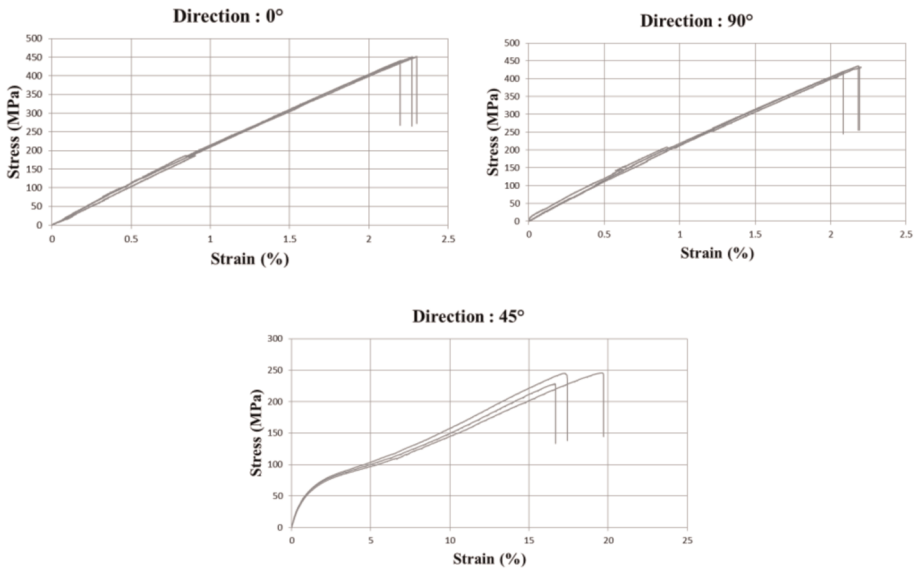

Figure 5. Material responses from tensile tests in 0°, 90°, and 45° directions

To model such a material behavior, we adopted the classical metallic plasticity theory for anisotropic material to model this non-linear behavior, which is called "pseudo-plasticity". The Hill's yield criterion is the simplest yield criterion for anisotropic material, which reduces to von Mises criterion when the anisotropy is considerably small.

$$F(\sigma_{22}-\sigma_{33})^2+G(\sigma_{33}-\sigma_{11})^2+H(\sigma_{11}-\sigma_{22})^2+2L\sigma_{23}^2+2M\sigma_{31}^2+2N\sigma_{12}^2=1 \quad (3)$$

$$2F=\frac{1}{\sigma_{y,22}^2}+\frac{1}{\sigma_{y,33}^2}+\frac{1}{\sigma_{y,11}^2} \quad (4)$$

$$2G=\frac{1}{\sigma_{y,23}^2}+\frac{1}{\sigma_{y,11}^2}+\frac{1}{\sigma_{y,22}^2} \quad (5)$$

$$2H=\frac{1}{\sigma_{y,11}^2}+\frac{1}{\sigma_{y,22}^2}+\frac{1}{\sigma_{y,33}^2} \quad (6)$$

$$2L=\frac{1}{\tau_{y,23}^2} \quad (7)$$

$$2M=\frac{1}{\tau_{y,13}^2} \quad (8)$$

$$2N=\frac{1}{\tau_{y,12}^2} \quad (9)$$

where σ_y and τ_y are respectively the tensile yield strength and the shear yield strength.

In this work, Hill's yield criterion was modified to yield only in the off-axis directions. Indeed, non-linear behavior is only contributed to the in-plane shear stress. Generally, the parameters of Hill's yield criterion (F, G, H, L, M, and N) are used to describe the current state of anisotropy, and can be determined from yield strengths of each stress components. Thus, to modify the Hill's yield criterion to yield only in the off-axis direction, all Hill's parameters except N, which describes yielding in the off-axis direction, were determined from the corresponding failure strengths to ensure that

there is no plasticity contributed by these components. For yielding in the off-axis direction described by the parameter N, the yield shear strength was determined experimentally from the tensile tests in 45° direction. The results of Hill's yield criterion parameters are summarized in the table 2.

Table 2. Parameters of Hill's yield criterion

F	G	H	L	M	N
51.96×10^{-7}	48.82×10^{-7}	1.08×10^{-7}	2.94×10^{-4}	2.67×10^{-4}	67×10^{-4}

Furthermore, the plastic flow was also determined from tensile tests in 45° direction and modeled by non-linear isotropic hardening model in which its monotonic loading response can be represented by:

$$\sigma_{eq,y} = \sigma^0_{eq,y} + H\varepsilon^P_{eq}\left(1 - e^{-b\varepsilon^P_{eq}}\right) \tag{10}$$

where $\sigma^0_{\text{eq.y}} = 15$, $H = 880$, $Q = 37$, $b = 300$. The 2D numerical simulations were conducted on Abaqus in the fiber direction (0°) and off-axis direction (45°), compared to the experiments as shown in figure 6.

4. Open-hole specimen

In this section, the prediction of failure load in composite plates containing an open-hole is presented. As mentioned in the earlier section that a non-uniform stress distribution caused by stress concentration leads to the underestimation of failure load predicted by local failure criteria. In order to overcome this issue, we propose here the method of non-localized approach. The experimental tests were first conducted to determine the characteristic volume by the aide of numerical simulation, and then the

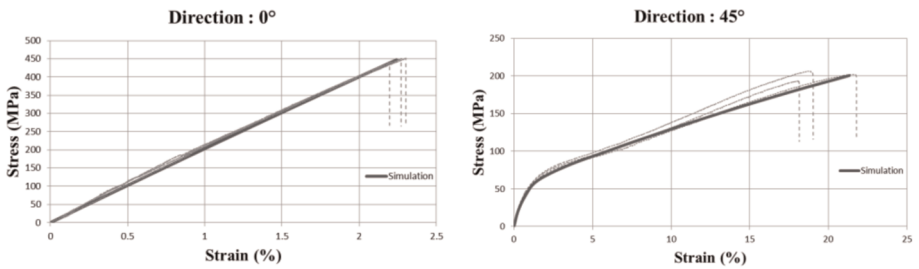

Figure 6. Comparison of simulations and experimental results in fiber and off-axis directions for tensile tests

failure loads of other specimens with different configurations were numerically predicted and compared with experimental results as a validation of proposed method.

4.1. Experiments

The test procedure was guided by ASTM D5766. All open-hole specimens used in this work have the same width of 50 mm. However, different in hole diameter and material orientation as summarized in table 3. Tensile tests on open-hole specimens were carried out by Instron universal testing machine. The extensometer and video extensometer were used as observation methods. The failure mechanisms involving these open-hole specimens were matrix cracking, delamination, fiber re-orientation, and fiber tow fracture (Belmonte *et al*., 2001, 2004). The results of failure strengths are also shown in the table 3.

Table 3. Open-hole specimen configurations and results of failure strength

Configuration	Width, W (mm)	Diameter, D (mm)	D/W	Orientation[a]	Strength (MPa)
W50D3	50	3	0.06	0°	270.91
W50D6.8	50	6.8	0.14	0°	192.28
W50D6.8-15	50	6.8	0.14	15°	136.59
W50D6.8-30	50	6.8	0.14	30°	118.77
W50D6.8-45	50	6.8	0.14	45°	141.00
W50D10	50	10	0.20	0°	177.44

a. Orientations of the fibers.

The experimental stress-strain curves are presented in the figure 7. The effect of hole size is shown in the figure 7a, when keeping the specimen width constant at 50 mm. As mentioned by Collings (1977), more stress relief takes place around the hole for smaller hole diameter resulting in higher failure strength. In the figure 7b, the specimens with the same geometry (width of 50 mm and hole diameter of 6.8 mm) but different according to fiber material orientation are plotted together. The results showed that the failure strengths in the fiber direction (0°) and in the off-axis directions (15°, 30°, and 45°) were considerable different due to the different failure mechanisms. In the fiber direction the specimens were failed by fiber breaks, while in the off-axis directions fiber reorientations took place before fracture of fiber tows resulting in significant non-linear behavior, *i.e.* lower strength and higher strain.

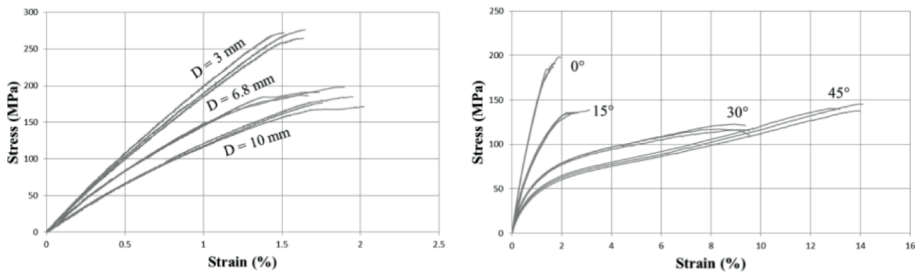

(a), 0° (b), hole 6.8mm

Figure 7. (a) Comparison of 50-mm width open-hole specimens with different hole sizes; (b) comparison of open-hole specimens with the same geometry but different in material orientation

4.2. Numerical simulations

The 2D numerical simulations of open-hole specimen were conducted on Abaqus with introduction of plasticity mentioned in the section 3 as a validation of material behavior. Meshes of all specimen configurations were created and loaded up to failure for each configuration. Figure 8 shows the comparison of numerical and experimental results of the configuration W50D6.8 with four different material orientations; 0°, 15°, 30°, and 45°.

From the results shown in figure 8, the simulations have a good agreement with experiments except in the direction 15°. This is due to the fact that the non-linear behavior described by classical plasticity theory cannot take into account all of non-linear contributions, especially the fiber reorientations of composite loaded in off-axis direction, which is locally appeal and more severe in the direction 15°. As shown in

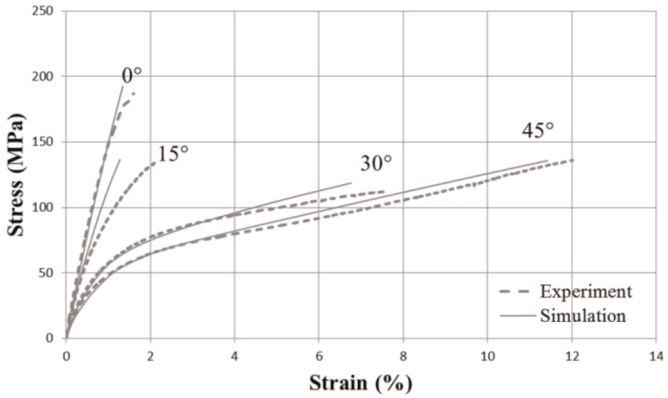

Figure 8. Numerical simulations of W50D6.8 with different material orientations against experiments

figure 9, the fibers in weft direction tried to locally reorient and distort toward loading direction resulting in superior elongation at break compare to the simulations.

4.3. Post-processing for failure prediction

To predict the specimen failure, the stress fields around the hole of each configuration were exported from Abaqus using Abaqus scripting interface for post-processing in Matlab. A python script was written to create the zone of interest around the hole, and then write all stress components at the integration points situated in the zone of interest as a function of spatial coordinates in a text file.

The failure criteria used in this work are the maximum stress criterion (equation (10)) and Hashin failure criteria, generally used to predict the failure of unidirectional composites. Thus, for woven composites, only tensile and compressive fiber failures are applied to the warp and the weft directions as stated in equations (11) and (12) for the warp direction (the failures in all material orientations 0°, 15°, 30°, and 45° were clearly due to the fiber breaks, figure 9).

Maximum stress criterion, MSTRS:

$$MSTRS = \max\left(\frac{\sigma_{11}}{S_{11}}, \frac{\sigma_{22}}{S_{22}}, \frac{\sigma_{33}}{S_{33}}, \frac{\sigma_{12}}{S_{12}}, \frac{\sigma_{13}}{S_{13}}, \frac{\sigma_{23}}{S_{23}}\right) \tag{11}$$

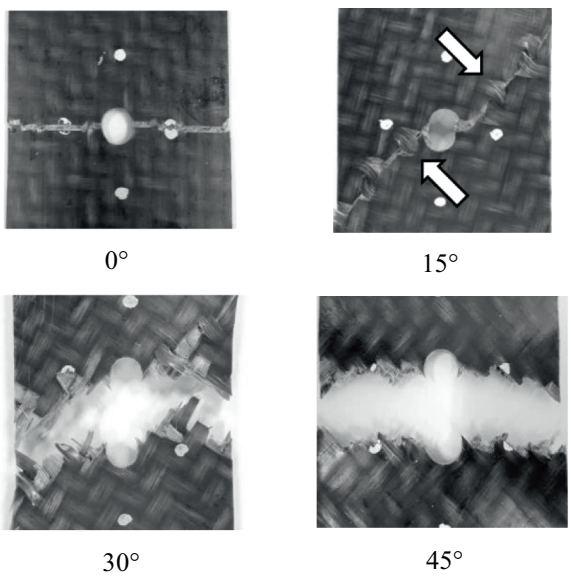

Figure 9. W50D6.8 specimens with different material orientations at failure

Hashin tensile fiber failure criterion, HSNFTCRT ($\sigma_{11} \geq 0$):

$$HSNFTCRT = \left(\frac{\sigma_{11}}{S_{11T}}\right)^2 + \left(\frac{\tau_{12}}{S_{12}}\right)^2 + \left(\frac{\tau_{13}}{S_{13}}\right)^2 \quad (12)$$

Hashin compressive fiber failure criterion, HSNFCCRT ($\sigma_{11} < 0$):

$$HSNFTCRT = \left(\frac{\sigma_{11}}{S_{11C}}\right)^2 \quad (13)$$

where:

- S_{11T}, S_{11C}: tensile and compressive strength in the warp direction;
- S_{22T}, S_{22C}: tensile and compressive strength in the weft direction;
- S_{12}, S_{13}, S_{23}: the shear strengths;
- S_{11} equals S_{11T} for $\sigma_{11} \geq 0$ and equals S_{11C} for $\sigma_{11} < 0$;
- S_{22} equals S_{22T} for $\sigma_{22} \geq 0$ and equals S_{22C} for $\sigma_{22} < 0$.

In Matlab, all stress components at each integration point were imported as well as their corresponding coordinates to determine failure indices of maximum stress and Hashin failure criteria at each point. Then, an average value of failure indices inside the characteristic volume which is reduced from a cylinder to a circle for 2D problem can be determined by equation (1) with area, A instead of volume, V. This characteristic circle sweeps around the hole edge to determine and locate the maximum average value of failure indices, as shown in figure 10. Finally, the diameter of characteristic circle, D_c was determined from the diameter that delivers the average failure index, $\overline{FI} = 1$.

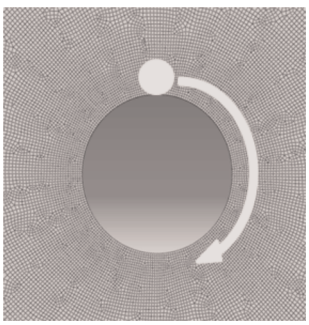

Figure 10. Maximum average failure parameters are determined by sweeping the characteristic circle around the hole edge

Table 4. Results of average failure parameters for each specimen configuration

Configuration	Maximum stress criterion		Hashin failure criteria	
	$\overline{FI}_{\text{MSTRS}}$	% error	$\overline{FI}_{\text{HSNCRT}}$	% error
W50D3	1.10	10	1.27	27
W50D6.8[a]	1.00	0	1.00	0
W50D6.8-15	0.95	5	0.98	2
W50D6.8-30	0.98	2	1.44	44
W50D6.8-45	0.97	3	1.29	29
W50D10	1.02	2	1.04	4

a. W50D6.8 is the reference geometry used to determine the characteristic diameter.

4.4. Results and discussions

The characteristic diameters, D_c for maximum stress criterion (MSTRS) and Hashin failure criteria (HSNCRT) were first determined from the specimen configuration W50D6.8 which is 0° orientation, and equaled to 0.61 mm. and 0.68 mm, respectively. Then, $D_{\text{c.MSTRS}} = 0.61$ and $D_{\text{c.HSNCRT}} = 0.68$ were used to predict failure of other configurations. The simulated stress fields around the hole at failure of other configurations were then exported for post-processing. The results of average failure indices, $\overline{FI}_{\text{MSTRS}}$ and $\overline{FI}_{\text{HSNCRT}}$, determined by $D_{\text{c.MSTRS}}$ and $D_{\text{c.HSNCRT}}$, are shown in the table 4.

From the results shown in table 4, the maximum failure criterion is more suitable to predict the failure using the non-localized approach with maximum error of 10%, while the Hashin failure criteria resulted in maximum error of 44%. This can be explained by the squared term in the mathematical expressions of Hashin failure criteria. For material direction 0° where the shear stress does not exist, the $D_{\text{c.HSNCRT}}$ shown less errors but, for other configurations, the errors increase exponentially due to the squared term of normal stress component. For other material directions where the shear stress is more elevated, the failure index is the combination of normal and shear components, which results in overestimation up to 44% error.

5. Application on bolted composite joint

This section presents how the proposed method applied on the bolted composite joint to predict its failure. Since the material model used in this work does not take into account the damage evolution during analysis, the predicted failure is consequently a damage onset of the join. Experimental studies on bolted composite join were first

conducted to determine the bearing responses of the join as well as a damage initiation. Then, numerical simulations were used to predict the failure of bolted composite join.

5.1. Experiments

The specimens had the width of 41 mm, a hole diameter of 6.8 mm, and the distance between the hole and the end edge of 41 mm, as shown in figure 11a. The geometry of specimens was chosen in order to obtain the bearing failure mode as proposed by Collings (1977). Furthermore, the specimens were fabricated in two material orientations; 0° and 45°. The test procedure was guided by ASTM D5961 and the specimen deformations were measured by digital image correlation through a series of images, figure 11b. Note that, due to the fixture proposed by ASTM D5961, only the deformation at the specimen edge can be measured (figure 11c), where the distance between observation points was 20 mm, as shown in figure 11d.

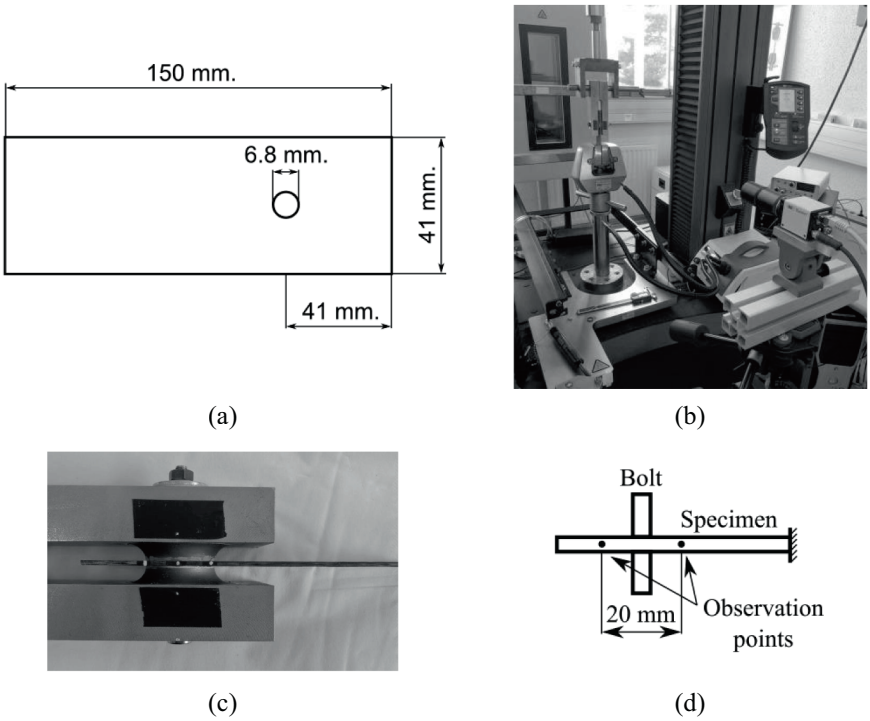

Figure 11. (a) Bolted composite join geometry; (b) experimental setup for bearing response test; (c) test fixture according to ASTM D5961; (d) distance between observation point

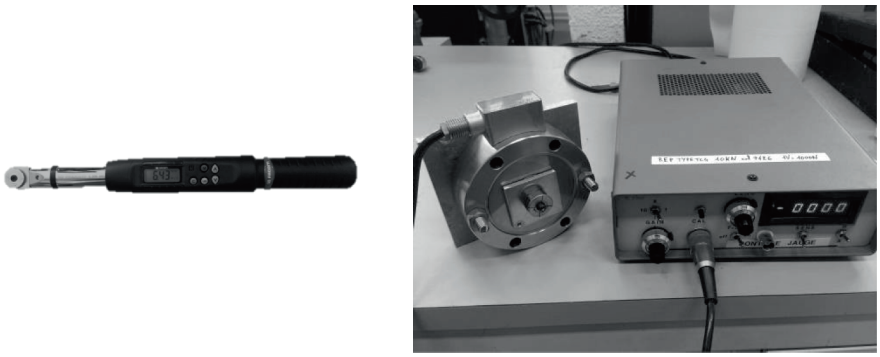

(a) (b)

Figure 12. (a) 8-Nm torque was applied by a torque wrench; (b) clamping force was measured by a load cell with a simple setup

In this work, experiments were carried out on two material orientations (0° and 45°) with two clamping conditions (hand-tight and controlled torque of 8 Nm), resulting in four test configurations. The torque of 8 Nm was applied using a torque wrench providing a clamping force about 8 kN, calculated in Annexe 1appendix 1, and measured by a load cell (figure 12b), whereas a hand-tight condition gives only 90 N of clamping force.

To determine bearing response of the composite in both material orientations, the specimens were loaded until the bearing failure took place. In the fiber direction (0°), the bearing loads of both clamping conditions remain nearly identical, even the bearing failure onset was delayed by the effect of clamping force, as shown in figure 13a. While, in the 45° direction, the bearing loads were obviously increased when the clamping force was applied (figure 13b). At curves beginning, the increase do not exactly corresponds to the initial friction force as in metallic assemblies, because we have relaxation in the

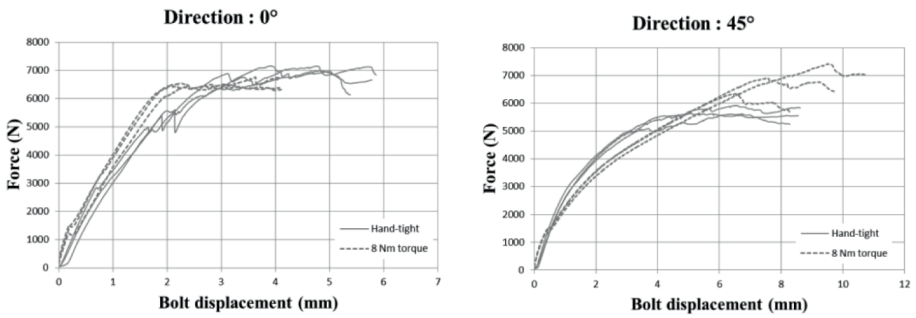

(a) (b)

Figure 13. Comparison of bearing responses for hand-tight and 8-Nm torqued conditions: (a) in the fiber direction 0°; (b) in the 45° direction

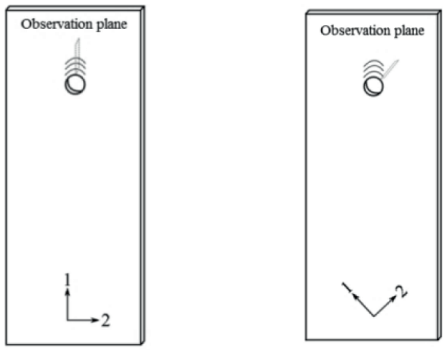

Figure 14. Observation planes of 0° and 45° specimens

composite (Annexe 2appendix 2). For 45° direction, the increase affects essentially the maximum reached force.

After obtaining the bearing responses of the composite in 0° and 45° directions for both clamping conditions, the damage initiations due to the local compressive failure, which is considered as a primary failure mechanism (Wu and Sun, 1998), were determined by the observations through a microscope for each test configuration. The specimens were loaded to various load levels and then observed through a microscope. The observation planes for 0° and 45° material orientations are shown in the figure 14. The observation results are shown in the figures 15-18 for all four test configurations.

From the observations on the specimens in the 0° direction, the local compressive failure was found at the load of 4,000 N which means that the damage onset took place between 3,500-4,000 N for the hand-tight condition (figure 15). After applying a torque of 8 Nm, we also observed the local compressive failure on the fiber at 4,000 N, except

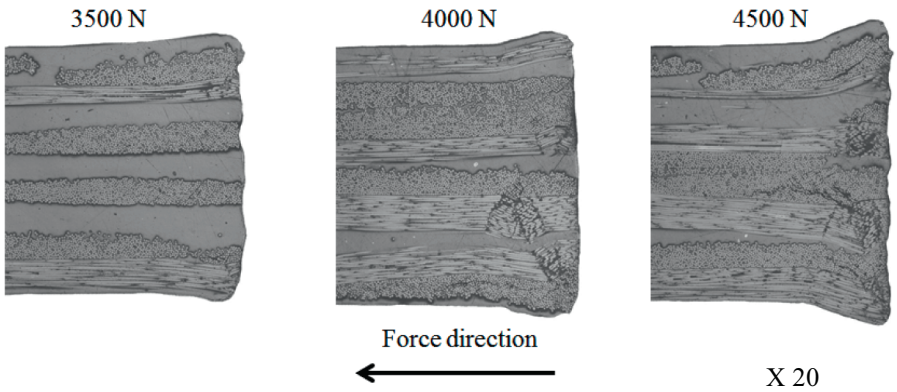

Figure 15. Damage initiation was found at 4,000 N for specimen in 0° direction with hand-tight condition

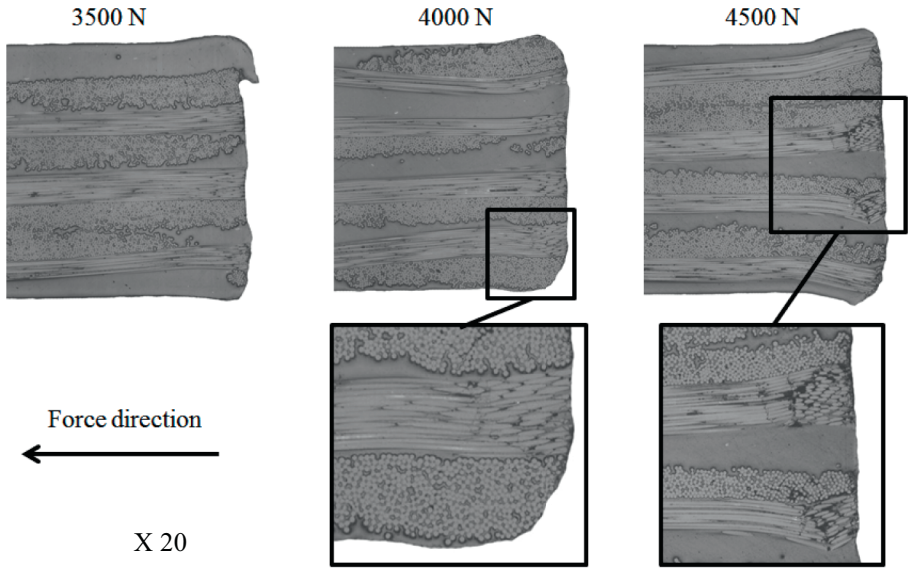

Figure 16. Damage initiation was found to be starting at 4,000 N, and obviously found at 4,500 N for specimen in 0° direction with torque of 8 Nm

that the fibers were less damaged (figure 16). For the specimens in 45° direction, the damage initiation was found on some specimens at 5,000 N for the hand-tight condition (figure 17). Then, for the 8-Nm torqued specimens, the damage was still found at the load of 5,000 N with less damages compared to the hand-tight condition (figure 18).

From the experiments on the four test configurations of bolted composite joint, we conclude that the clamping force slightly delay the damage initiation for the bolted

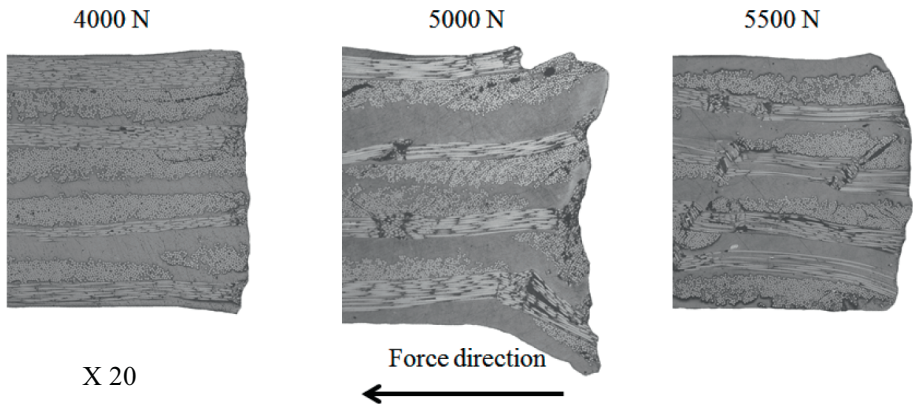

Figure 17. Damage initiation was found at 5,000 N for specimen in 45° direction with hand-tight condition

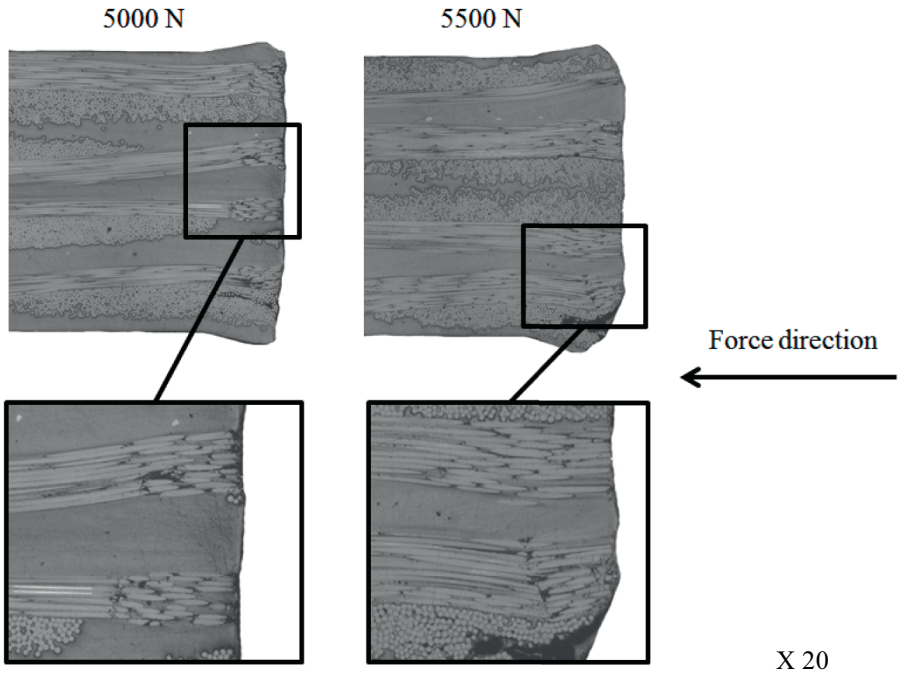

Figure 18. Damage initiation was also found at 5,000 N for specimen in 45° direction with torque of 8 Nm

composite joint in both 0° and 45° cases since the observations shown less damage at the same load level. In order to study the effect of clamping force in more details, the observations at refined loading step should be performed while varying an applied torque. However, due to the availability of material, the further study on this effect has not performed in this work.

Concerning to the load at bearing failure, the clamping force can generally delay the delamination resulting in an improved bearing failure load. From the results of the experiments performed in this work, the load is improved in the case of 45° specimens but remains the same in the case of 0° specimen after applying a torque of 8 Nm. For the 0° specimens, this can be explained by the fact that, on the zone subjected to the tensile load, the material cross-sectional area (both the width and the thickness) was reduced as well as its volume since the Poisson's ratios is less than 0.5.

Therefore, the effect of clamping force was also progressively reduced as the specimen deformed, due to the fact that after the torque of 8 Nm was reached, there was no clamping force control during the experiment. In the case of 45° specimens, the specimens were principally subjected to the shear loads due to material orientation, and were consequently deformed with volume constant, which means that the effect of clamping force was maintained during the experiments resulting in the improvement of the load at bearing failure for the 45° specimens.

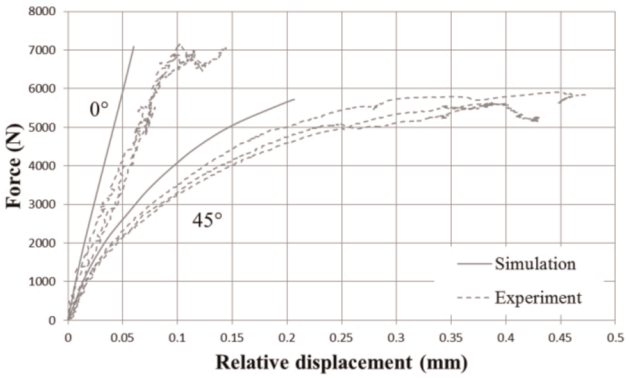

Figure 19. Numerical simulations of bolted composite joints in the 0° and 45° directions against experiments

5.2. Failure predictions

The damage initiation of the bolted composite was determined, as presented in the previous section, which shows that the application of clamping force can slightly improve the damage initiation. However, since the improvement is rather small and the effect of clamping force not well known, the numerical simulations on the bolted composite joint were conducted on Abaqus software without considering the clamping force to determine the failure of the specimens in both material orientations (0°, 45°). The simulation results are shown in the figure 19, where the relative displacement is the displacement between two observation points at the specimen edge (figure 11d). These relative displacements obtained from simulations were smaller than the relative displacements measured experimentally due to the fact that the Young's modulus in compression is about 12% higher than the tensile Young's modulus, as shown in table 1, and this phenomenon cannot be taken into account by the material in the used model. Indeed, at the contact between the composite and the bolt, this zone is stiffer since it is loaded in compression. While at the specimen edge, where the displacement was measured, the composite is loaded in tension resulting in larger deformation than the simulation.

To determine the failure of bolted composite joint in both material directions, the post-processing proposed in the section 4 was carried out. Since the results from maximum stress criterion were better, only this failure criterion was applied. The failure index was calculated according to the equation (10) to determine the load giving the maximum stress failure index equal to unity. At $\overline{FI}_{\mathrm{MSTRS}} = 1$, which is contributed by the compressive component in the equation (10), the obtained failure loads were 3,600 N and 4,900 N for the material orientation of 0° and 45°, respectively. This is in agreement with the failure initiation determined experimentally, which were less than 4,000 N for the 0° direction and about 5,000 N for the 45° direction.

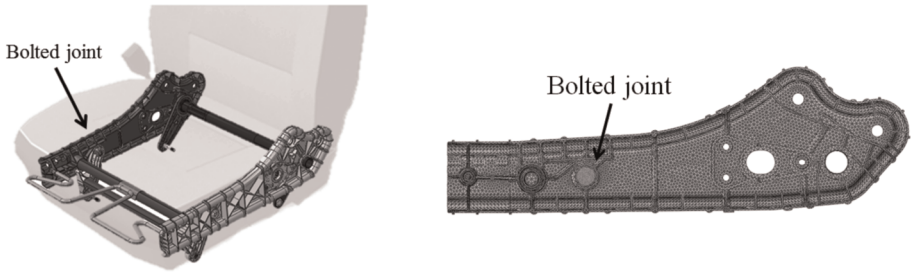

Figure 20. Mesh of the composite automotive seat provided by Faurecia partner

6. Application on the multi-material structure

This work was developed for the project designing a composite automotive seat using multi-material structure. The tests on a prototype were carried out by the industrial partner. The measured force acting on the bolted composite joint was provided to use in this study. Note that a bolt hole was fabricated by piercing the composite sheet and forming the edge in the out of plane direction (figure 21), which aims to reinforce the hole comparing to a drilled hole resulting in an improved strength. The specimens with this "pierced hole" were fabricated by the industrial partner with a hole diameter of 6.8 mm and a width of 50 mm. This is the reason where the reference geometry of the open-hole specimen originates from.

The mechanical tests on these specimens showed an increase in the strength of an open-hole specimen about 19% as demonstrated by the normalized strengths in the

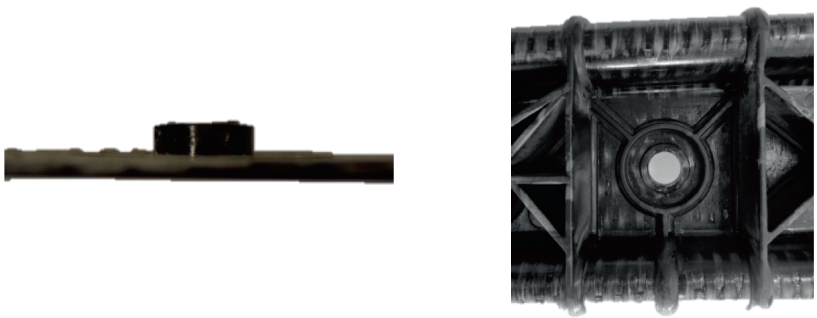

(a) (b)

Figure 21. Pierced hole: (a) on a specimen; (b) on the industrial structure (top view)

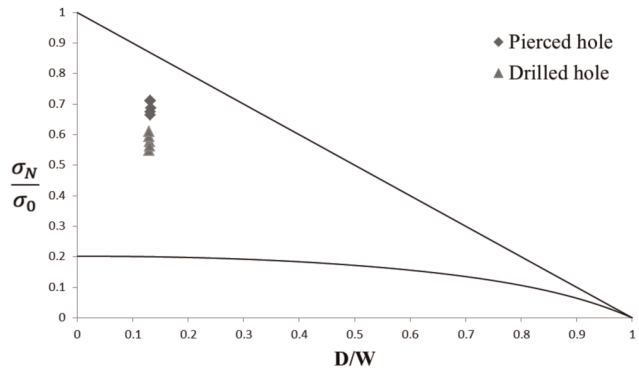

Figure 22. Comparison of normalized strengths of open-hole specimens with a drilled hole and a pierced hole

figure 22, where σ_N is the open-hole strength and σ_0 is the material strength. Since, in this work, the availability of specimens with pierced hole is very limited, to take into account the improvement in strength of the open-hole specimen with a pierced hole, the material strength defining in the maximum stress criterion was adjusted while the characteristic diameter $D_{c.MSTRS}$ remains the same. To determine an increase in material strength due to the pierced hole, the numerical simulations on a specimen with a drilled hole were carried out using the failure load of the specimen with a pierced hole, and then, the post-processing was performed to determine the material strength resulting in $\overline{FI}_{MSTRS} = 1$. As a result, the failure of the specimens with pierced hole can be predicted by increasing the material strength by 17%. Therefore, the material tensile and compressive strengths used to determine the failure of the bolted joint on the industrial structure were also increased by 17% and using a drilled hole instead of a real geometric pierced hole in order to take into account this improvement in strength even though the improvement in compressive strength has not been studied due to the specimen availability.

The numerical simulations were conducted on Abaqus finite element code using the geometry (figure 20) provided by the industrial partner. The boundary conditions were applied to impose the provided load to the bolted composite joint, as shown in the figure 23a-b. The mechanical properties of the composite proposed in the section 3 and other materials in the seat structure were used to complete the model. The mesh around the hole was refined until the mesh independence was obtained. Also shown in the figure 23c is the resulting contour plot of von Mises around the hole.

To determine the failure due to the applied loading, the stress field around the hole was exported for post-processing in Matlab. Since the analysis of the structure is three-dimensional, the characteristic circle becomes the characteristic volume. In this work, this characteristic volume has a cylindrical shape with the diameter determined in the section 4, while the volume thickness was chosen to equal to the composite thickness.

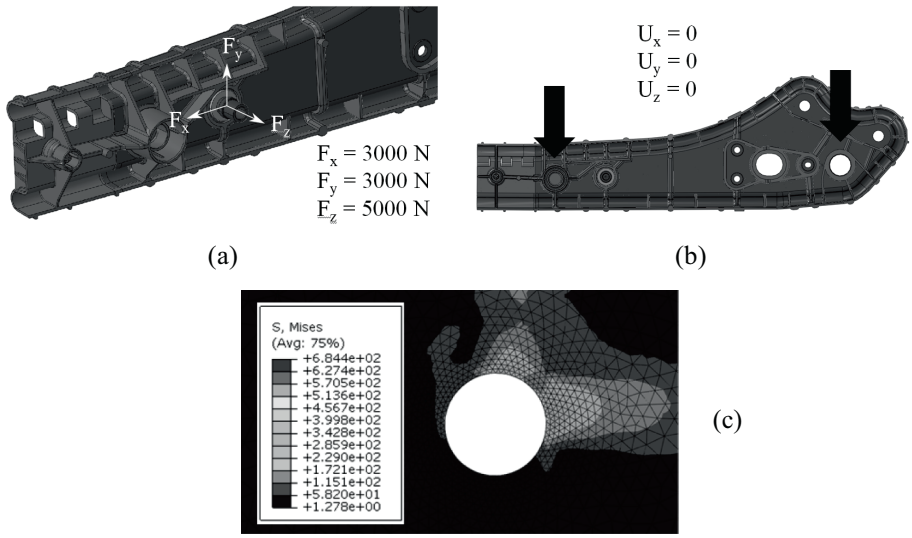

Figure 23. (a) Applied forces on the bolted composite join measured during the tests; (b) other joints on the structure were imposed by zero displacements; (c) contour plot of von Mises stress around the hole

The resulting maximum average failure index in the characteristic volume was 0.62, which was in agreement with the test result that the bolted joint of the seat has not been broken. Further analyses were conducted to determine the load that is sufficient to fail the bolted composite joint. After applying the factor 1.55 to the load measured from the test, the failure condition $\overline{FI}_{\mathrm{MSTRS}} = 1$ was obtained. This implies that the bolted composite joint of the prototype would fail at $F_x = 4{,}650\,\mathrm{N}$, $F_y = 4{,}650\,\mathrm{N}$, and $F_z = 7{,}750\,\mathrm{N}$.

7. Conclusions

The twill glass/polyamide 6 composite has been modeled using Hill's yield criterion in combination with the non-linear isotropic hardening model to describe the non-linear behavior of the material when loaded in off-axis direction. Tensile, compressive, bending and Arcan-Mines tests were carried out to determine all engineering constants as well as the non-linear parameters, which represent the material responses in the fiber direction and the off-axis directions, as shown in the figure 6. The characteristic diameter was first determined from the tensile tests on open-holed specimens with the reference geometry by aided simulation. Then, the numerical simulations were conducted to predict the failure of specimens with smaller and larger hole of diameters and with different material orientations as a validation of the proposed method. The results show a good agreement with the experiments using maximum stress criterion.

Mechanical tests on the bolted composite joint were also carried out with two clamping conditions; hand-tight condition and 8-Nm torqued condition. For the

specimen in 0° direction, the application of 8-Nm torque slightly increases the damage initiation load from between 3,500-4,000 N to 4,000 N as can be seen by the observations through a microscope (figures 15-16), while the loads at bearing failure of both clamping conditions still remain the same. For the specimen in 45° direction, the damage initiations were found about 5,000 N for both clamping conditions, whereas the load at bearing failure was increased about 30%. To predict the failure of these bolted composite joints, the proposed method was used to determine the damage initiation of the joints for both material directions, which were 3,600 N and 4,900 N for 0° and 45° directions, respectively. The proposed method is able to predict a local failure initiation as shown by the microscopic observations that the damage onset was found on its fibers at the load predicted by the proposed method. This satisfies the industrial requirement that the damage is not supposed to exist in the material. The proposed method was also applied to determine the failure of the industrial structure and showed a good agreement with the test results that the structure did not fail at the given load condition.

Appendix 1: Relation between torque and clamping force in the bolted assembly

The clamping force is obtained with a tightening with a torque wrench. We establish the relation between clamping force and torque tightening.

When we screw the nut with an angle $\Delta\theta$, we develop in the screw a force F and an elongation Δl. We have also additional frictions:

- in the thread between nut and screw;
- between the surface washer and the nut.

If we consider the energetic balance, the work of the clamping torque C gives the elongation of the screw (traction work), and overcome the friction work (between nut and screw, between screw and washer) (figure 24).

With the energetic work of the torque: $W = C\ \Delta\theta$, given to the assembly, we write the assessment, with a friction coefficient f:

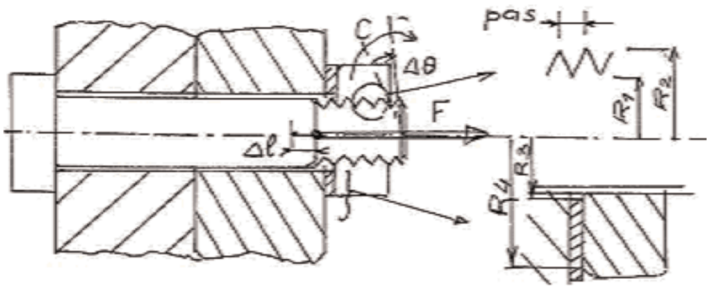

Figure 24. Diagram of the energetic tightening balance

$$W = C\Delta\theta = F\Delta l + \Delta\theta \int_{R_1}^{R_2} \frac{F}{\pi\left(R_2^2 - R_1^2\right)} f 2\pi r^2 \, dr + \Delta\theta \int_{R_3}^{R_4} \frac{F}{\pi\left(R_4^2 - R_3^2\right)} f 2\pi r^2 \, dr \qquad (14)$$

with: $\Delta 1 = t\frac{\Delta\theta}{2\pi}$, t is the thread of the screw.

Finally:

$$F = \frac{C}{\frac{t}{2\pi} + \frac{2}{3} f \frac{\left(R_2^3 - R_1^3\right)}{\left(R_2^2 - R_1^2\right)} + \frac{2}{3} f \frac{\left(R_4^3 - R_3^3\right)}{\left(R_4^2 - R_3^2\right)}} \qquad (15)$$

In our case, $t = 1.00$ mm, $R_1 = 2.459$, $R_2 = 3.00$, $R_3 = 3.20$, $R_4 = 5.00$.

For $f = 0.12$ (friction steel on lubricated steel), $F = 1.0187$ C.

Appendix 2: Initial friction force in the tightened assembly

When we have a clamping force F in the tightened assembly, with a friction coefficient f^* between steel and composite, the initial friction force is $T = f^*F$. This value is supported in traction by the assembly before bolt displacement in the assembly.

If we have $F = 8$ kN, with $f^* = 0.25$ (steel-composite friction coefficient), we calculate $T = 2$ kN. In fact, we measure for T a 10 lower value (figure 13). The origin of this lake is the relaxation in composite before the test. This is a fundamental difference with metallic assembly: we do not have a mechanical connection by friction between the parts but by shearing of the bolt.

Acknowledgements

We would like to express our gratitude to ADEME for supporting this work through the project DEMOS (DEsign and Manufacturing of cOmposite interior Structure).

Bibliographie

Belmonte H.M.S., Manger C.I.C., Ogin S.L., Smith P.A., Lewin R. (2001). Characterization and modeling of the notched tensile fracture of woven quasi-isotropic GFRP laminates. *Composites Science and Technology*, vol. 61, p. 585-597.

Belmonte H.M.S., Ogin S.L., Smith P.A., Lewin R. (2004). A physically-based model for the notched strength of woven quasi-isotropic CFRP laminates. *Composites Part A: Applied Science and Manufacturing*, vol. 35, p. 763-778.

Choi J.H., Chun Y.J. (2003). Failure load prediction of mechanically fastened composite joints. *Journal of Composite Materials*, vol. 37, p. 2163-2177.

Collings T.A. (1977). *The strength of bolted joints in multi-directional CFRP laminates*. Her Majesty's Stationary Office.

Duthinh D. (2000). *Connections of fiber-reinforced polymer (FRP) structural members: a review of the state of the art*. Structural Division, Building and Fire Research Laboratory, NIST, Gaithersburg, MD.

Gay D. (2005). *Matériaux composites*. Hermès.

Hochard C., Lahellec N., Bordreuil C. (2007). A ply scale non-local fiber rupture criterion for CFRP woven ply laminated structures. *Composite Structures*, vol. 80, p. 321-326.

Miot S., Hochard C., Lahellec N. (2010). A non-local criterion for modeling unbalanced woven ply laminates with stress concentrations. *Composite Structures*, vol. 92, p. 1574-1580.

Nelson W.D., Bunin B.L., Hart-Smith L.J. (1983). *Critical joints in large composite aircraft structure*. NASA Contractor report 3710, Scientific and Technical Information Branch.

Patamaprohm B., *et al*. (2016). Study of adhesive joints under static and fatigue loading. *Revue des composites et des matériaux avancés*, vol. 26, n° 1, p. 63-86.

Rösch J. (1995). Modeling the mechanical properties in polypropylene/polyamide-6 blends with core shell morphology. *Polymer Engineering & Science*, vol. 35, p. 1917-1922.

Tan S.C. (1988). Effective stress fracture models for unnotched and notched multidirectional laminates. *Journal of Composite Materials*, vol. 22, p. 322-340.

Wang J., Callus P.J., Bannister M.K. (2004). Experimental and numerical investigation of the tension and compression strength of un-notched and notched quasi-isotropic laminates. *Composite Structures*, vol. 64, p. 297-306.

Whitney J.M., Nuismer R.J. (1974). Stress fracture criteria for laminated composites containing stress concentrations. *Journal of Composite Materials*, vol. 8, p. 253-265.

Wu P.S., Sun C.T. (1998). Modeling bearing failure initiation in pin-contact of composite laminates. *Mechanics of Materials*, vol. 29, p. 325-335.